Text S1: Supplementary Information

Modeling dynamics of cell-to-cell variability in TRAIL-induced apoptosis explains fractional killing and reversible resistance

François Bertaux, Szymon Stoma, Dirk Drasdo, Gregory Batt

Supplementary Results

Biochemistry of TRAIL-induced apoptosis

The activation of the death receptor DR4/5 by TRAIL binding promotes the assembly of the death-inducing signaling complexes (DISC), which recruit and activate initiator caspases like caspase-8 (C8) [sup. ref. 1]. Once activated, initiator caspases cleave and activate effector caspases such as caspase-3 (C3). Effector caspases cleave essential structural proteins, inhibitors of DNase, and DNA repair proteins (PARP), eventually leading to cell death. The cellular effect of effector caspase activation is regulated by factors such as XIAP, which blocks the proteolytic activity of caspase-3 by binding tightly to its active site and promotes its degradation via ubiquitination [sup. ref. 2]. In addition to the direct activation of effector caspases, initiator caspases also activate Bid and Bax [sup. ref. 3]. If not kept in check by inhibitors, most notably Bcl2, activated Bax directly contributes to the formation of pores in the mitochondria outer membrane, leading to MOMP [sup. ref. 4]. Following MOMP, critical apoptosis regulators, such as Smac and cytochrome c (CyC), translocate into the cytoplasm. Smac binds to and inactivates XIAP, thus relieving the inhibition of effector caspases by XIAP [sup. ref. 5]. Cytochrome c combines with Apaf-1 to form the apoptosome that in turn activates the initiator caspase-9 (C9) that activates effector caspases. A simplified view is given in Fig. S1.

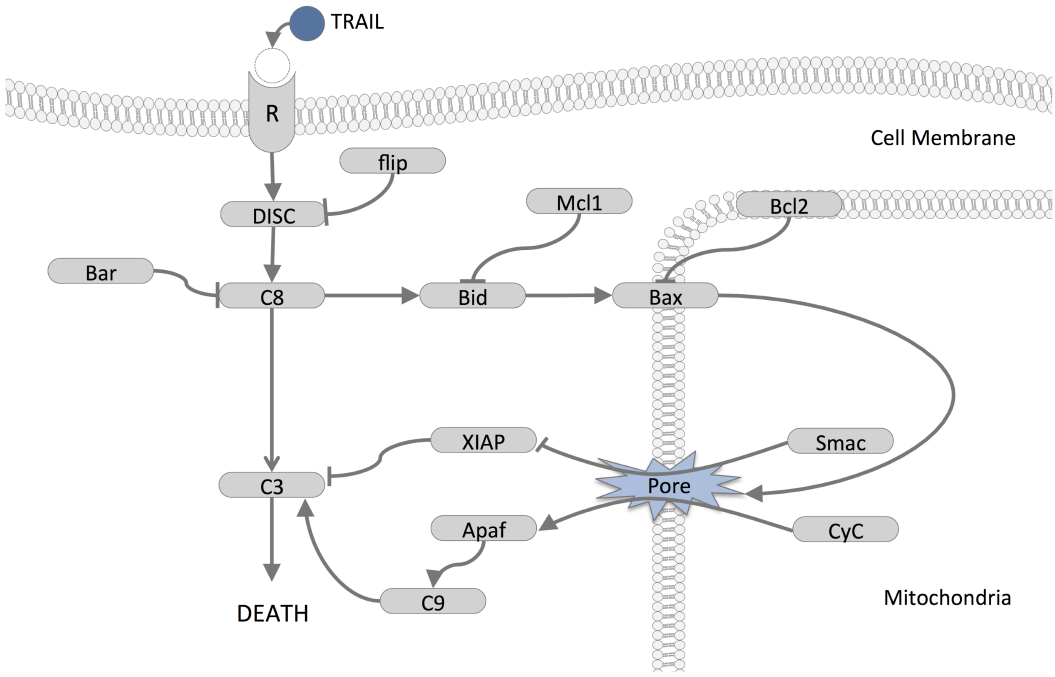

Figure S1: Simplified view of the TRAIL-induced apoptosis pathway. Only the type of each protein-protein interaction (activation or inhibition) is represented. A diagram displaying the detail of protein complexes and activated forms can be find in [5].

Modeling stochastic protein turnover

We model protein turnover with a stochastic process describing mRNA level fluctuations (promoter activity switches, mRNA production and degradation are stochastic events), and deterministic processes for protein translation and degradation (Fig. S2).

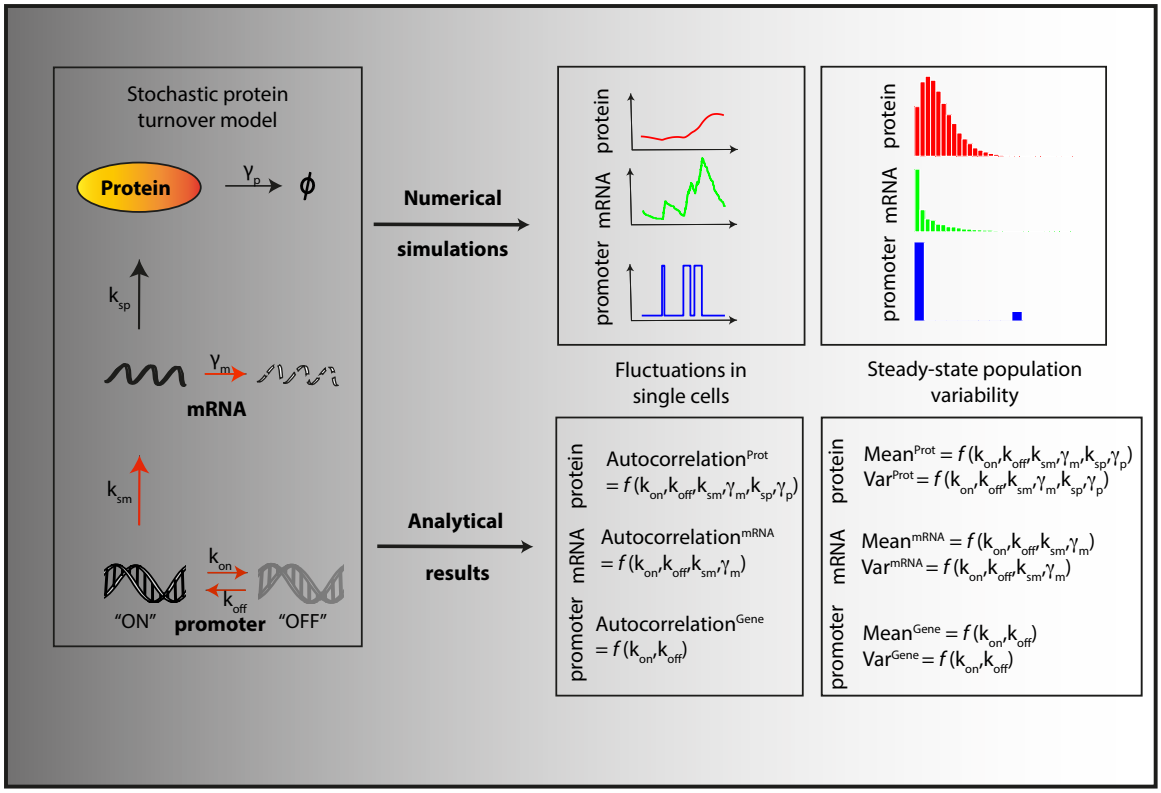

Figure S2: Numerical simulation and analytical characterization of stochastic protein turnover models. A stochastic protein turnover model is defined by six rates: the promoter activity switching rates, the mRNA production and degradation rates, the protein per mRNA synthesis rate and the protein degradation rate. Numerical simulations can be used to simulate temporal fluctuations in single cells. When a population of cells is simulated, the cell-to-cell variability can be studied. After some time, cell-to-cell variability reaches a steady state. Analytical calculations on the stochastic protein turnover model provide expressions characterizing the steady-state variability (moments of the steady-state distributions), but also fluctuations (autocorrelation functions). Complete expressions are given in Text S1.

To constrain model rates based on experimentally available information, one can use analytical expressions characterizing steady-state mRNA and protein level distributions (moments) and their fluctuations (autocorrelations functions). The derivation of steady-state

distribution moments can be done by performing Laplace transforms (equivalently referred as generating functions) on the steady-state formulation of the chemical master equation. The obtained system of equations is closed because there are no reactions of order 2 or higher. It has been done by Paszek [39] and yields for example the following moments for the steady-state distribution:

- Promoter activity (denoted by G, equal to either 0 or 1)
  - $\mathbb{E}\left[G\right] = \frac{k_{on}}{k_{on}+k_{off}} = \frac{k_{on}}{\gamma_g} \qquad \left(\gamma_g = k_{on}+k_{off}\right)$
  - $Var\left[G\right] = \mathbb{E}\left[G\right]\left(1-\mathbb{E}\left[G\right]\right)$
  - $CV\left[G\right]^2 = \frac{Var\left[G\right]}{\mathbb{E}\left[G\right]^2} = \frac{1-\mathbb{E}\left[G\right]}{\mathbb{E}\left[G\right]}$
- mRNA level (denoted by m, taking discrete values)
  - $\mathbb{E}\left[m\right] = \mathbb{E}\left[G\right]\frac{k_{sm}}{\gamma_m}$
  - $Var\left[m\right] = \frac{\gamma_m}{\gamma_m+\gamma_g} CV\left[G\right]^2 \mathbb{E}\left[m\right]^2 + \mathbb{E}\left[m\right]$
  - $CV\left[m\right]^2 = \frac{\gamma_m}{\gamma_m+\gamma_g} CV\left[G\right]^2 + \frac{1}{\mathbb{E}\left[m\right]}$
- Protein level (denoted by P, taking continuous values)
  - $\mathbb{E}\left[P\right] = \mathbb{E}\left[m\right]\frac{k_{sp}}{\gamma_p}$
  - $Var\left[P\right] = \frac{\gamma_p\gamma_m\left(\gamma_p+\gamma_m+\gamma_g\right)}{\left(\gamma_m+\gamma_p\right)\left(\gamma_m+\gamma_g\right)\left(\gamma_p+\gamma_g\right)} CV\left[G\right]^2 \mathbb{E}\left[P\right]^2 + \frac{\gamma_p}{\gamma_m+\gamma_p}\frac{\mathbb{E}\left[P\right]^2}{\mathbb{E}\left[m\right]}$
  - $CV\left[P\right]^2 = \frac{\gamma_p\gamma_m\left(\gamma_p+\gamma_m+\gamma_g\right)}{\left(\gamma_m+\gamma_p\right)\left(\gamma_m+\gamma_g\right)\left(\gamma_p+\gamma_g\right)} CV\left[G\right]^2 + \frac{\gamma_p}{\gamma_m+\gamma_p}\frac{1}{\mathbb{E}\left[m\right]}$

We now present the derivation of the autocorrelation function. The first step is to obtain the differential equations describing the temporal evolution of the first moments. Such equations are obtained by using the master equation, which gives how the joint probability distribution

$p^t\left(G=g, m=x, P=y\right)$ is changed during an infinitesimal time interval dt because of the reactions that can occur:

$$\frac{dp^{t+dt}\left(g,x,y\right)}{dt}=\left[k_{off}\left(1-g\right)+k_{on}g\right]p^t\left(1-g,x,y\right)+k_{sm}g\,p^t\left(g,x-1,y\right)$$
$$+\gamma_m\left(x+1\right)p^t\left(g,x+1,y\right)+k_{sp}x\,p^t\left(g,x,y-1\right)+\gamma_p\left(y+1\right)p^t\left(g,x,y+1\right)$$
$$-\left[k_{on}\left(1-g\right)+k_{off}g+k_{sm}g+\gamma_m x+k_{sp}x+\gamma_p y\right]p^t\left(g,x,y\right)$$

For example, if one is interested in the temporal evolution of $\mathbb{E}\left[G\right]$:

$$\frac{d\mathbb{E}\left[G\right]}{dt}=\frac{d\left(\sum_{g,x,y}gp^t\left(g,x,y\right)\right)}{dt}$$
$$=\sum_{g,x,y}g\frac{d\left(p^t\left(g,x,y\right)\right)}{dt}$$
$$=\sum_{g,x,y}g\left[k_{off}\left(1-g\right)+k_{on}g\right]p^t\left(1-g,x,y\right)+k_{sm}g^2p^t\left(g,x-1,y\right)$$
$$+g\gamma_m\left(x+1\right)p^t\left(g,x+1,y\right)+gk_{sp}x\,p^t\left(g,x,y-1\right)+g\gamma_p\left(y+1\right)p^t\left(g,x,y+1\right)$$
$$-g\left[k_{on}\left(1-g\right)+k_{off}g+k_{sm}g+\gamma_m x+k_{sp}x+\gamma_p y\right]p^t\left(g,x,y\right)$$

Noticing that $g\left(1-g\right)=0$, $g^2=g$ and that the probability distribution cannot charge states where $x=-1$ or $y=-1$, one gets:

$$\frac{d\mathbb{E}\left[G\right]}{dt}=k_{on}\sum_{g,x,y}gp^t\left(1-g,x,y\right)-k_{off}\sum_{g,x,y}gp^t\left(g,x,y\right)$$
$$=k_{on}\left(1-\mathbb{E}\left[G\right]\right)-k_{off}\mathbb{E}\left[G\right]$$
$$=k_{on}-\gamma_g\mathbb{E}\left[G\right]$$

With similar calculations, one also obtains the two following equations:

$$\frac{d\mathbb{E}\left[m\right]}{dt}=k_{sm}\mathbb{E}\left[G\right]-\gamma_m\mathbb{E}\left[m\right]$$

$$\frac{d\mathbb{E}\left[P\right]}{dt}=k_{sp}\mathbb{E}\left[m\right]-\gamma_p\mathbb{E}\left[P\right]$$

This system of autonomous ordinary differential equations is linear and can be solved analytically. In particular, we have:

$$\mathbb{E}\left[P\right]\left(t+T\right)=f\left(t,\mathbb{E}\left[G\right]\left(T\right),\mathbb{E}\left[m\right]\left(T\right),\mathbb{E}\left[P\right]\left(T\right)\right)$$

$$=\mathbb{E}\left[G\right]\left(T\right)c_G\left(t\right)+\mathbb{E}\left[m\right]\left(T\right)c_m\left(t\right)+\mathbb{E}\left[P\right]\left(T\right)c_P\left(t\right)+c_0\left(t\right)$$

where:

$$c_P\left(t\right)=e^{-\gamma_p t}$$

$$c_m\left(t\right)=\frac{\mathbb{E}_{eq}\left[P\right]}{\mathbb{E}_{eq}\left[m\right]}\left\{e^{-\gamma_m t}-e^{-\gamma_p t}\right\}$$

$$c_G\left(t\right)=\frac{\mathbb{E}_{eq}\left[P\right]}{\mathbb{E}_{eq}\left[G\right]}\frac{\gamma_m\gamma_p}{\left(\gamma_p-\gamma_m\right)\left(\gamma_m-\gamma_g\right)\left(\gamma_p-\gamma_g\right)}\left\{\left(\gamma_m-\gamma_g\right)e^{-\gamma_p t}+\left(\gamma_g-\gamma_p\right)e^{-\gamma_m t}+\left(\gamma_p-\gamma_m\right)e^{-\gamma_g t}\right\}$$

$$c_0\left(t\right)=\mathbb{E}_{eq}\left[P\right]-\mathbb{E}_{eq}\left[P\right]c_P\left(t\right)-\mathbb{E}_{eq}\left[m\right]c_m\left(t\right)-\mathbb{E}_{eq}\left[G\right]c_G\left(t\right)$$

This particular ordering has been chosen to facilitate the next step of the auto-correlation function derivation, which is to find an appropriate expression for the quantity $\mathbb{E}_{eq}\left[P\left(t\right)P\left(0\right)\right]$:

$$\mathbb{E}_{eq}\left[P\left(t\right)P\left(0\right)\right]=\sum_{g_0,x_0,y_0}\sum_{g,x,y}yy_0\mathbb{P}\left(\begin{array}{c|c}G\left(t\right)=g & G\left(0\right)=g_0\\ m\left(t\right)=x & m\left(0\right)=x_0\\ P\left(t\right)=y & P\left(0\right)=y_0\end{array}\right)\mathbb{P}_{eq}\left(g_0,x_0,y_0\right)$$

letting the expectation of $P\left(t\right)$ when starting from a dirac in $\left(g_0,x_0,y_0\right)$ at $t=0$ appear:

$$=\sum_{g0,x0,y0}y_0\mathbb{E}\left(\begin{array}{c|c}P\left(t\right) & G\left(0\right)=g_0\\ & m\left(0\right)=x_0\\ & P\left(0\right)=y_0\end{array}\right)\mathbb{P}_{eq}\left(g_0,x_0,y_0\right)$$

$$=\sum_{g0,x0,y0}y_0f\left(t,g_0,x_0,y_0\right)\mathbb{P}_{eq}\left(g_0,x_0,y_0\right)$$

$$=\sum_{g0,x0,y0}\left[y_0g_0c_G\left(t\right)+y_0x_0c_m\left(t\right)+{y_0}^2c_P\left(t\right)+y_0c_0\left(t\right)\right]\mathbb{P}_{eq}\left(g_0,x_0,y_0\right)$$

letting crossed second order moments of the steady-state distribution appear:

$$=\mathbb{E}_{eq}\left[GP\right]c_G\left(t\right)+\mathbb{E}_{eq}\left[mP\right]c_m\left(t\right)+\mathbb{E}_{eq}\left[P^2\right]c_P\left(t\right)+\mathbb{E}_{eq}\left[P\right]c_0\left(t\right)\mathbb{E}_{eq}\left[P\right]$$

We thus have:

$$\mathbb{E}_{eq}\left[P(t)P(0)\right]-\mathbb{E}_{eq}\left[P\right]^2 = Var(P)c_P(t)+Cov(m,P)c_m(t)+Cov(G,P)c_G(t)$$

and therefore:

$$A\left[P\right](t)=\frac{\mathbb{E}_{eq}\left[P(t)P(0)\right]-\mathbb{E}_{eq}\left[P\right]^2}{Var(P)}=c_P(t)+\frac{Cov(m,P)}{Var(P)}c_m(t)+\frac{Cov(G,P)}{Var(P)}c_G(t)$$

Finally, after having plugged the expressions for the covariances (given in [39]) and for the functions $c_G(t), c_m(t)$ and $c_P(t)$, we get a final expression (i.e. containing only terms for which expression in terms of rate parameters has been given already) for the autocorrelation function:

$$A\left[P\right](t)=e^{-\gamma_p t}+h_m(\gamma_m,\gamma_p,t)+\frac{1}{CV\left[P\right]^2}\frac{1-\mathbb{E}\left[G\right]}{\mathbb{E}\left[G\right]}\frac{\gamma_p\gamma_m}{(\gamma_m+\gamma_g)(\gamma_p+\gamma_g)}h_g(\gamma_g,\gamma_m,\gamma_p,t)$$

with:

$$h_m(\gamma_m,\gamma_p,t)=\frac{\gamma_p}{\gamma_p-\gamma_m}\left\{e^{-\gamma_m t}-e^{-\gamma_p t}\right\}$$

$$h_g(\gamma_g,\gamma_m,\gamma_p,t)=\frac{\gamma_p\gamma_m}{(\gamma_p-\gamma_m)(\gamma_m-\gamma_g)(\gamma_p-\gamma_g)}\left\{(\gamma_m-\gamma_g)e^{-\gamma_p t}+(\gamma_p-\gamma_m)e^{-\gamma_g t}+(\gamma_g-\gamma_p)e^{-\gamma_m t}\right\}$$

The exactness of this expression was verified by Monte-Carlo simulations using Gillespie algorithm, for a parameter set carefully chosen such that each term in the expression has a non-negligible contribution to the function value. One can note how the three time-scales $\gamma_g,\gamma_m,\gamma_p$, corresponding to the promoter, the mRNA and the protein respectively, are convoluted together in this expression.

Short-lived protein fluctuations are more sensitive to bursting kinetics

Intuitively, fluctuations of short-lived proteins are expected to be more sensitive to the precise kinetics of bursting than long-lived proteins. Using protein level variability and half-autocorrelation time to characterize protein fluctuations, this hypothesis was confirmed from the corresponding analytical expressions (Fig. S3). This motivated us to consider standard stochastic protein turnover models for long-lived proteins but to give particular attention to the few short-lived proteins.

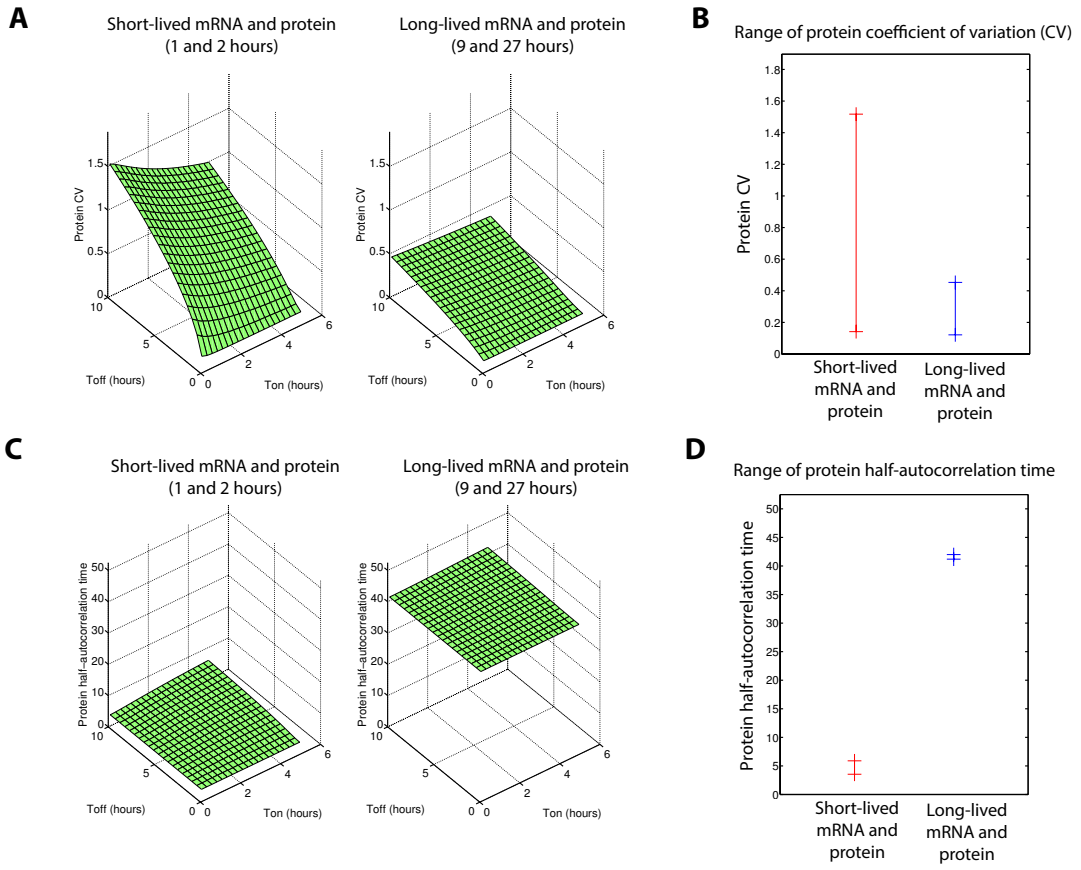

Figure S3: Fluctuations of protein levels caused by transcriptional bursting are smoothed out for long-lived proteins. Comparison of protein level coefficient of variation **(A)** and half-autocorrelation time **(C)** as a function of transcriptional bursting rates for two situations: a short-lived protein and mRNA (half-lives of 2 and 1 hours, resp.) and a long-lived protein and mRNA (27 and 9 hours, resp.). Other rates of the stochastic protein turnover model are chosen such that mean protein and mRNA level are the same (1000 and 17). Combinations of Ton and Toff values ranging from 0.1 to 5 hours and 0.1 to 10 hours respectively were tested. Ton and Toff are mean ON and OFF time of the gene. **(B and D)** Representation of the range of values obtained for all models tested in (A) and (C).

Modeling stochastic protein turnover in TRAIL-induced apoptosis

We apply our approach to TRAIL-induced apoptosis. We use EARM kinetic model [5,13] to describe protein-protein reactions taking place between TRAIL death exposure and cell death commitment. It comprises 17 native proteins and 41 other species involved in 71 reactions.

Unless required, we equipped all native proteins with the same default model of stochastic protein turnover. We used median values for mRNA levels, protein and mRNA half-lives from measured distributions in mammalian cells [sup.ref. 6]. At the promoter level, switching rates were estimated for a dozen of genes [36], and we used measured values to constrain

model reaction rates. Remaining rates were deduced from the mean and variance of protein level present as initial condition in [13] using analytical expressions derived from the stochastic protein turnover model (Fig. S4, Table S1).

As mentioned earlier, short-lived proteins should be given particular attention: transcriptional bursts are smoothed out in the fluctuations of a stable protein while fully revealed when both mRNA and protein exhibit fast turnover. Flip and Mcl1 are known to exhibit very fast turnover [42,43,44]. Measurements in mouse ES cells [sup. ref. 7] also suggest that Flip and Mcl1 transcripts are particularly short-lived. Therefore, we considered a specific stochastic protein turnover model for those two proteins, exploring realistic ranges for promoter switching rates, mRNA half-life and protein half-life (Fig. S4).

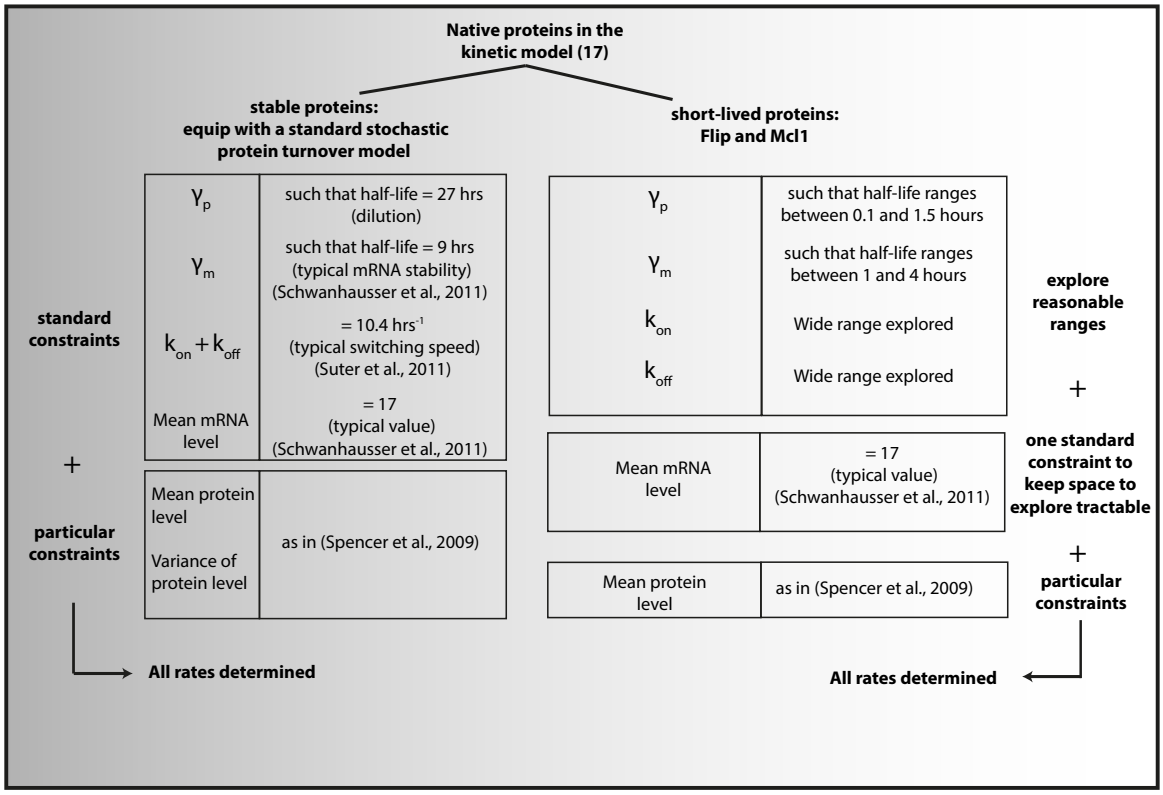

Figure S4: Building stochastic protein turnover models for TRAIL-induced apoptosis. Routine followed to choose rates of all 17 native proteins in the EARM kinetic model of TRAIL-induced apoptosis. Typical values from multi-genes studies in mammalian cells are used to constrain rate values. Specific attention is given to Flip and Mcl1 because they are known to be short-lived, and thus more prone to exhibit large variations.

Non-native protein species (catalytically activated forms or complexes) are also subjected to degradation. We used a half-life of 9 hours for TRAIL (as measured in [sup. ref. 8]), 1.9 hours for the mitochondrial pores (as in [13]) and the half-life of the native form for complexes involving Flip or Mcl1. For all other species we used a unique value (5 hours) to account for

the fact that active forms are usually degraded faster sup. refs. [9]-[13] values recapitulated in Table S3, see dedicated later section for discussion on the influence of this choice). We also assumed the feedback loop C3->C6->C8 to be absent (authors comment to [5], on editor's website). Otherwise, important cell death was still seen days after TRAIL treatment (see dedicated section for discussion on the feedback loop influence). It has been observed that protein synthesis is substantially decreased during apoptosis [sup. ref. 14]. Because this effect seems to happen essentially after effector caspases activation, when cells are already committed to death, we did not include it in our model.

Table S1. Standard stochastic protein turnover models

	Constraints				Rate values					
Protein	Switching speed $k_{on}+k_{off}$ (hrs^{-1}) [36] *fixed*	Mean mRNA level [sup. ref. 6, see Text S1] *fixed*	Mean protein level [13] *fixed*	Protein level Coefficient of Variation [13] *fixed*	Off to on promoter rate k_{on} (hrs^{-1}) *derived*	On to off promoter rate k_{off} (hrs^{-1}) *derived*	k_{sm} (min^{-1}) *derived*	mRNA deg. rate γ_m (hrs^{-1}) *fixed*	Protein synth. rate k_{sp} (min^{-1}) *derived*	Protein deg. rate γ_p (hrs^{-1}) *fixed*
Receptor	10.44	17	1000	0.25	0.388	10.05	0.587	0.077	0.025	0.0257
Caspase-8			10000	0.25	0.388	10.05	0.587		0.25	
Bar			1000	0.25	0.388	10.05	0.587		0.025	
Caspase-3			10000	0.282	0.289	10.15	0.789		0.25	
Caspase-6			10000	0.25	0.388	10.05	0.587		0.25	
XIAP			100000	0.288	0.275	10.17	0.829		2.52	
PARP			1000000	0.25	0.388	10.05	0.587		25.2	
Bid			60000	0.288	0.275	10.17	0.829		1.51	
Bax			80000	0.271	0.318	10.12	0.717		2.01	
Bcl-2			30000	0.294	0.268	10.18	0.871		0.76	
Pore			500000	0.25	0.388	10.05	0.587		12.6	
CytoC_m			500000	0.25	0.388	10.05	0.587		12.6	
Smac			100000	0.25	0.388	10.05	0.587		2.51	
Apaf			100000	0.25	0.388	10.05	0.587		2.51	
Caspase-9			100000	0.25	0.388	10.05	0.587		2.51	

Table S2. Specific stochastic protein turnover models

<u>"Non-fitted" model (Fig. S6):</u>

	Constraints		Rate values					
Protein	Mean mRNA level [sup. ref. 6, see Text S1]	Mean protein level [13]	k_{on} (hrs^{-1})	k_{off} (hrs^{-1})	k_{sm} (min^{-1})	γ_m (hrs^{-1})	k_{sp} (min^{-1})	γ_p (hrs^{-1})
Flip	17	2000	0.388	10.05	2.6186	0.3466	2.7182	1.39
Mcl-1	17	20000	0.388	10.05	2.6186	0.3466	27.182	1.39

"Fitted" model (Figs. 3,4,6,7):

	Constraints		Rate values					
Protein	Mean mRNA level [sup. ref. 6, see Text S1]	Mean protein level [13]	k_{on} (hrs^{-1})	k_{off} (hrs^{-1})	k_{sm} (min^{-1})	γ_m (hrs^{-1})	k_{sp} (min^{-1})	γ_p (hrs^{-1})
Flip	17	2000	0.0417	0.0625	0.4910	0.6931	3.3978	1.73
Mcl-1	17	20000	0.0417	0.0625	0.4910	0.6931	33.9780	1.73

Table S3. Non-native form degradation

Protein	Half-life (hours)	Reference
TRAIL	9	[sup. ref. 9, see Text S1]
Pore*	1.9	[13]
Flip:Receptor	same as Flip	
Mcl-1:tBid	same as Mcl-1	
All others	5	[sup. refs. 10-14, see Text S1]

Stochastic protein turnover models predicts transient memory in cell sensitivity to TRAIL and CHX

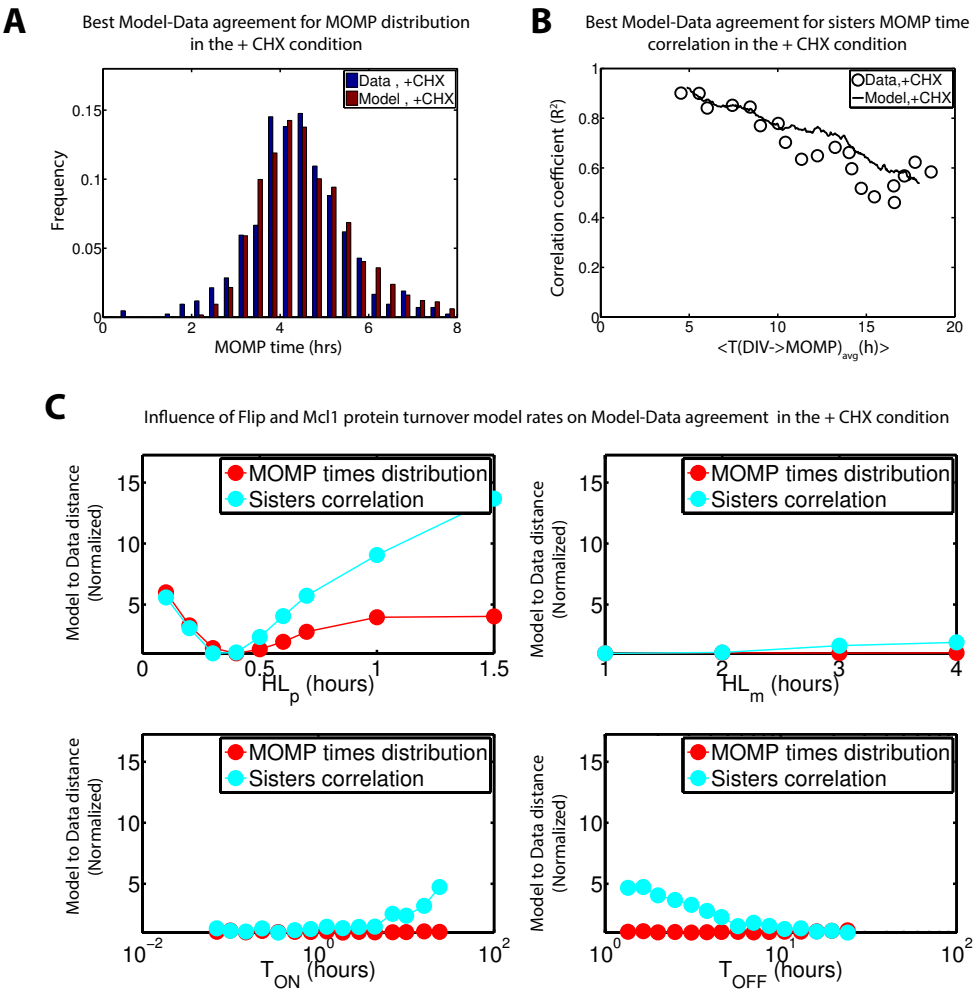

Figure S5: Stochastic protein turnover models captures fluctuations of cell sensitivity to TRAIL and CHX. **(A)** Best found agreement between model and data for MOMP times distribution in the +CHX condition. Obtained for Flip and Mcl1 model rates such that protein/mRNA half-life and mean ON/OFF promoter activity duration equaled 0.4/1 and 1.9/3.1 hours respectively. See Supplementary Methods (Text S1) for quantification of model data agreement. **(B)** Best found agreement between model and data for MOMP time correlation between sisters in the +CHX condition. Obtained for Flip and Mcl1 model rates such that protein/mRNA half-life and mean ON/OFF promoter activity duration equaled 0.3/1 and 0.35/24 hours respectively. **(C)** Influence of Flip and Mcl1 model rates on Model-Data agreement in the +CHX condition. For each parameter, we plot the model to data distance corresponding to the best model when all other three parameters are varied.

The "non-fitted" model quantitatively predicts TRAIL+CHX single-cell data and lead to fractional killing and reversible resistance for TRAIL alone treatments

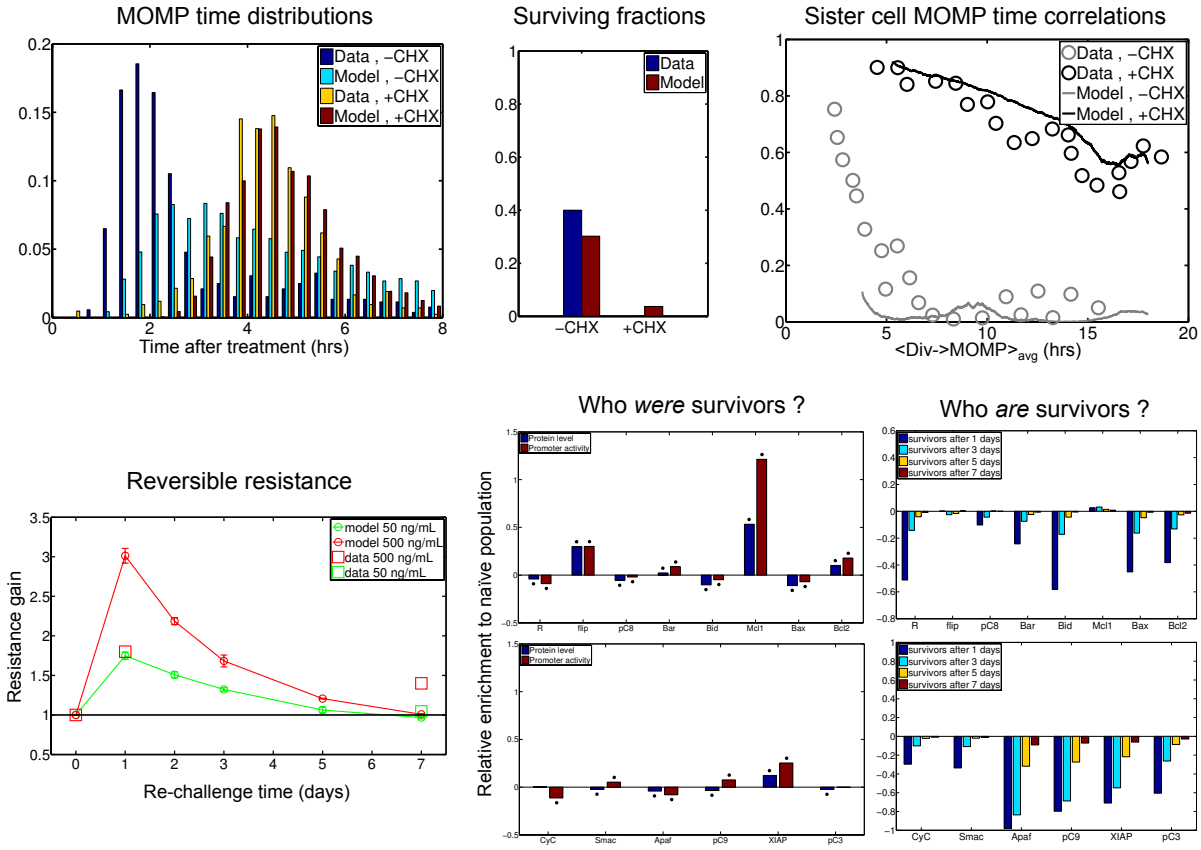

Figure S6: The "non-fitted" model quantitatively predicts TRAIL+CHX single-cell data and lead to fractional killing and reversible resistance for TRAIL alone treatments. In the non-fitted model, Flip and Mcl1 promoter switching rates are standard (Ton=0.1 hours and Toff=2.6 hours) but the short-half life of their mRNA and protein is accounted for (2 hours and 0.5 hours respectively). We reproduce here for this model all the results presented in the main text for the "fitted" model. Quantitative agreement is obtained for TRAIL+CHX single cell data from Spencer et al. [13] (MOMP time distribution and sister cell MOMP time correlations). No quantitative agreement is obtained in the case of TRAIL alone treatments, but the existence of fractional killing and reversible resistance is nevertheless predicted. Note that because fewer cells were simulated compared to main text figures (50000 instead of 10^5 for sister cell experiments), sister correlation curves appears slightly noisier.

Mcl1 and Flip fluctuations for the “non-fitted” and “fitted” model

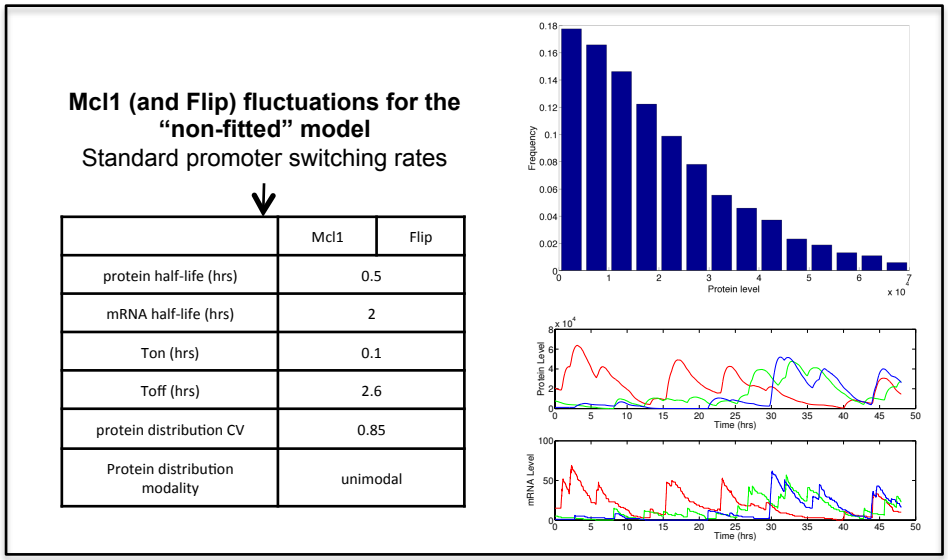

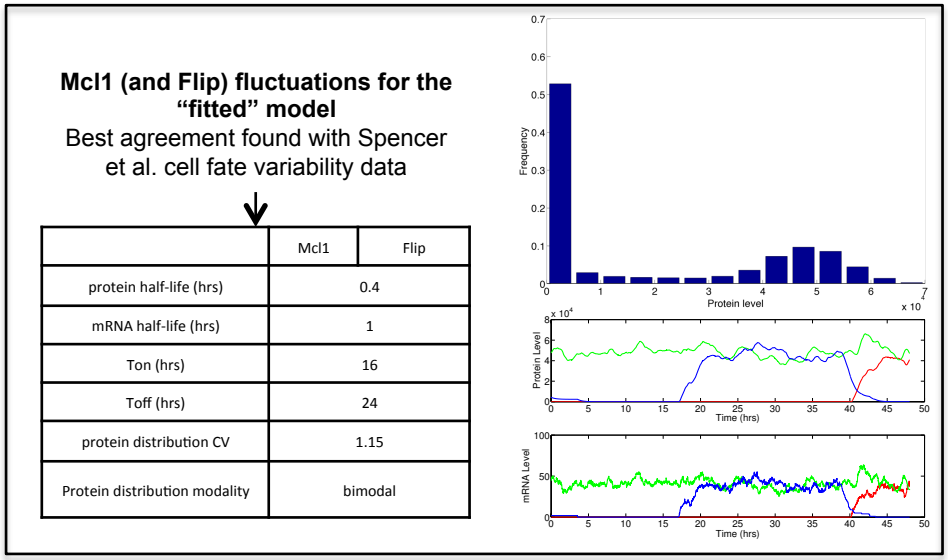

Figure S7: Mcl1 and Flip fluctuations for standard or “fitted” promoter switching rates. For the top frame, promoter switching rates are standard (as in Fig. 2). Because mRNA and protein half-lives are short, protein level fluctuates more rapidly and the steady-state distribution is changed (it is wider and the mode is in 0) compared to the standard stochastic protein turnover model (Fig. 2). On the bottom frame, the steady-state distribution becomes bimodal because the promoter switching rates are low compared to mRNA and protein degradation. In both cases, fluctuations and distribution are shown for Mcl1; they are similar for Flip as only the protein synthesis rate changes to account for a different mean protein level.

Large, rare fluctuations of Mcl1 alone are sufficient to explain cell fate variability and transient inheritance in both conditions

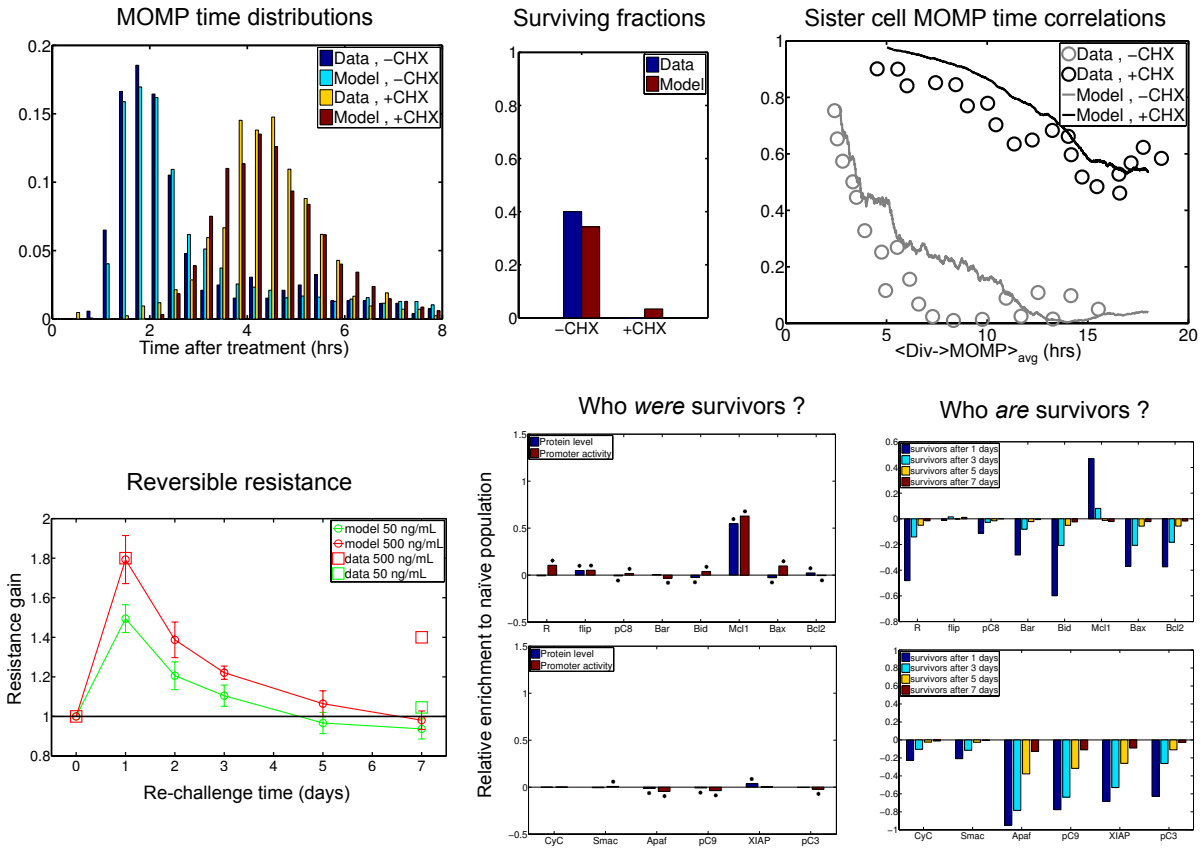

Figure S8: Large, rare fluctuations of Mcl1 alone are sufficient to explain cell fate variability and transient inheritance in both conditions. While Flip and Mcl1 protein and mRNA half-lives were the same as for the "fitted" model (0.4 and 1.0 hours respectively), only the Mcl1 promoter was assumed to have low switching rates (Ton and Toff are 16 and 24 hours resp.). The switching rates of the Flip promoter were assumed to be standard (Ton=0.1 hours and Toff=2.6 hours). All the results presented in the main text for the "fitted" model are reproduced here. Note that because fewer cells were simulated compared to main text figures (50000 instead of 10^5 for sister cell experiments), sister correlation curves appears slightly noisier.

Representative single-cell trajectories before and after TRAIL treatments

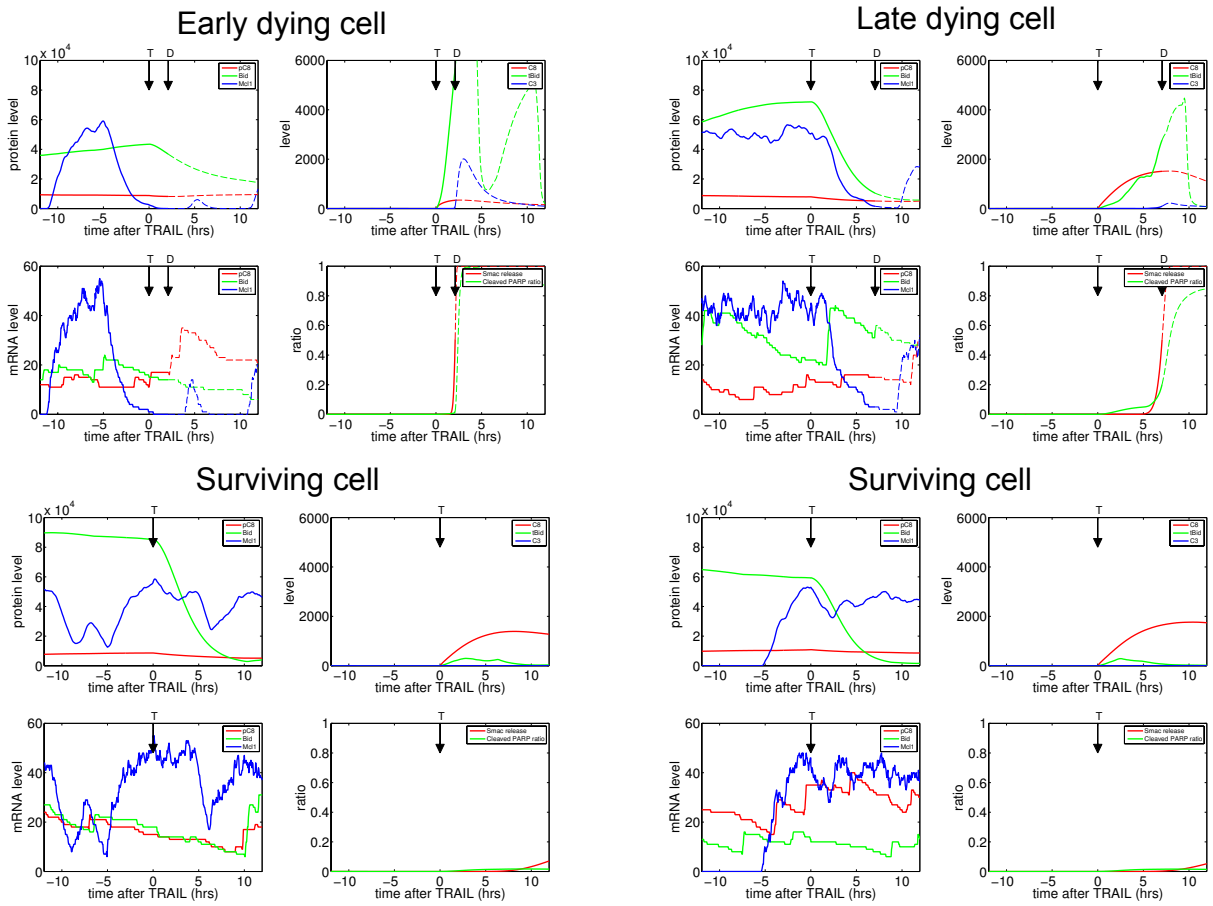

Figure S9: Representative single-cell trajectories before and after TRAIL treatment for the "fitted" model. Trajectories for two dying and two surviving cells (after 12 hours of TRAIL treatment) are shown. T-marked arrows denote the time of TRAIL addition (250 ng/mL), D-marked arrows denote the time of death commitment (MOMP). mRNA (lower left of each panel) and native form protein levels (upper left of each panel) are shown for pro-caspase 8, Bid and Mcl1. Levels of activated caspase 8, truncated Bid and activated caspase 3 are also shown (upper right of each panel), as well as the ratio of released Smac and of cleaved PARP (lower right of each panel).

Influence of C3->C6->C8 feedback loop and of non-native forms degradation

In presence of the feedback loop (as in the original model from Spencer et al., [13]) or with low degradation rates for non-native forms (also as in the original model), model predicts an extinction (or a non-reconstruction) of the cell number at 7 days after the treatment, in contradictions with observations.

Because the functional role of this feedback loop is debated (authors comment to [5], on editor's website) and non-native forms are often subjected to active degradation sup. refs. [9]-[13], we investigate whether realistic changes could re-conciliate the model with experimental observations.

We tested the effect of the presence/absence of the feedback loop as well as the influence of the value of the default non-native forms degradation rate (varied in a broad interval, between 2 to 27 hours in half-life). As shown in Figs. S10, S11 and S12, model predictions are remarkably robust, with the exception of population reconstruction after 7 days. This criterion led us, in the model, to assume that the feedback loop is absent and to use 5 hours as the default half-life of non-native forms.

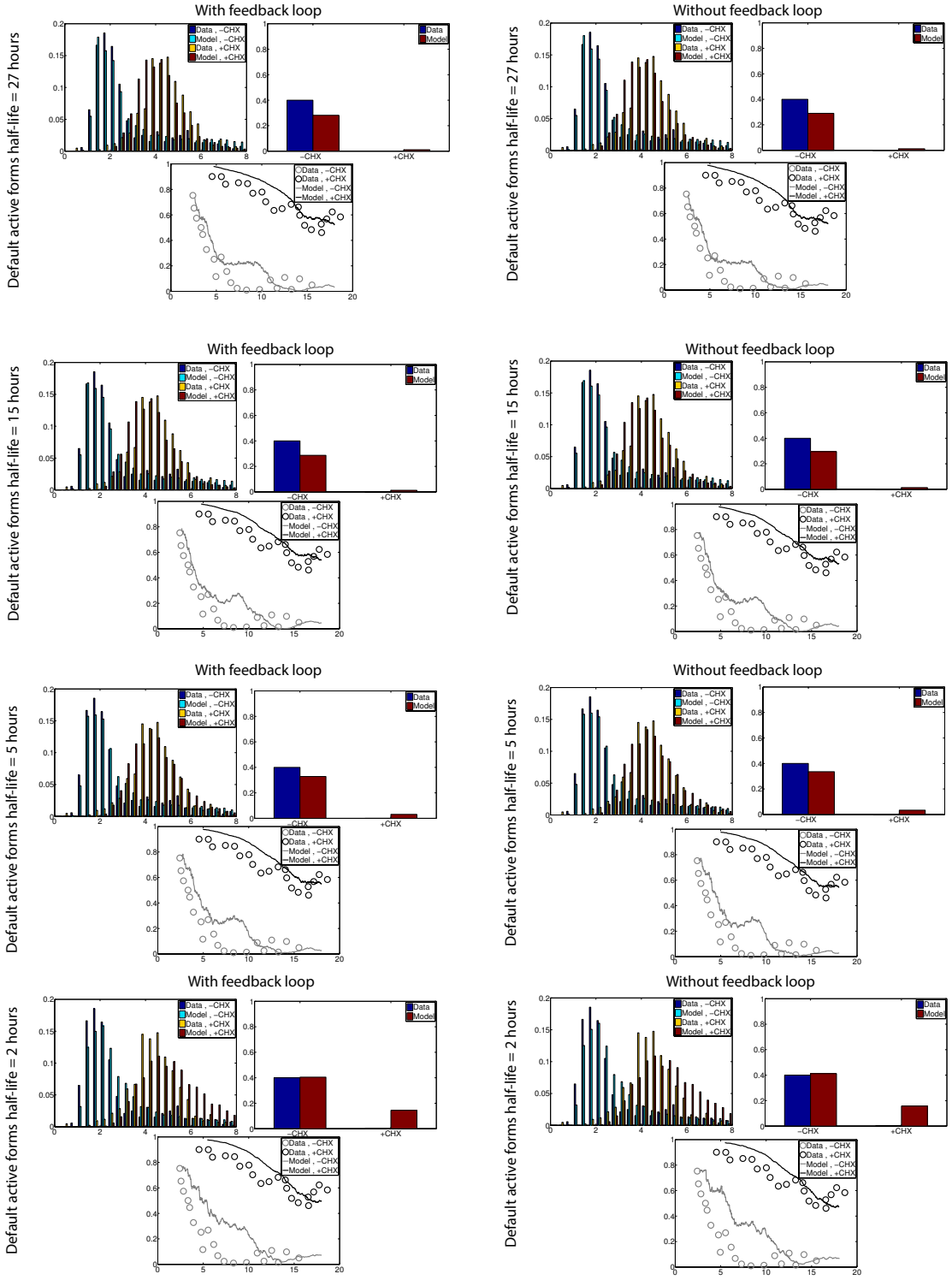

Figure S10: Robustness of short-term model behavior regarding the presence/absence of feedback loop and the degradation of active forms. Model-Data agreement is shown for MOMP time distributions, surviving fractions and sisters correlation of MOMP time in both treatment conditions for model variants when the C3->C6->C8 feedback loop is either present/absent and the default active forms half-life is 27, 15, 5 or 2 hours. Significant model-data deviation is seen only for the fastest active forms degradation.

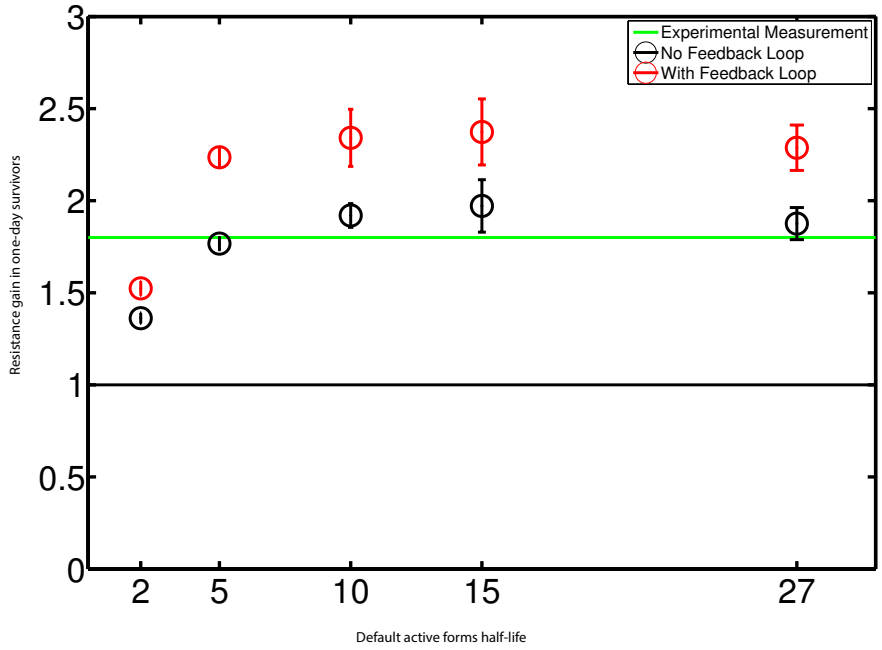

Figure S11: Resistance gain in one day survivors is robust regarding the presence/absence of feedback loop and the degradation of active forms. In-silico repeated TRAIL experiment (as in Fig. 6) was repeated for variants of the "fitted" model regarding presence/absence of the C3->C6->C8 feedback loop and the default active forms half-life. Resistance gain in one-day survivors is shown. Simulations were repeated 4 times with 10^4 cells, error bars indicate standard deviation of estimated resistance gain between replicates.

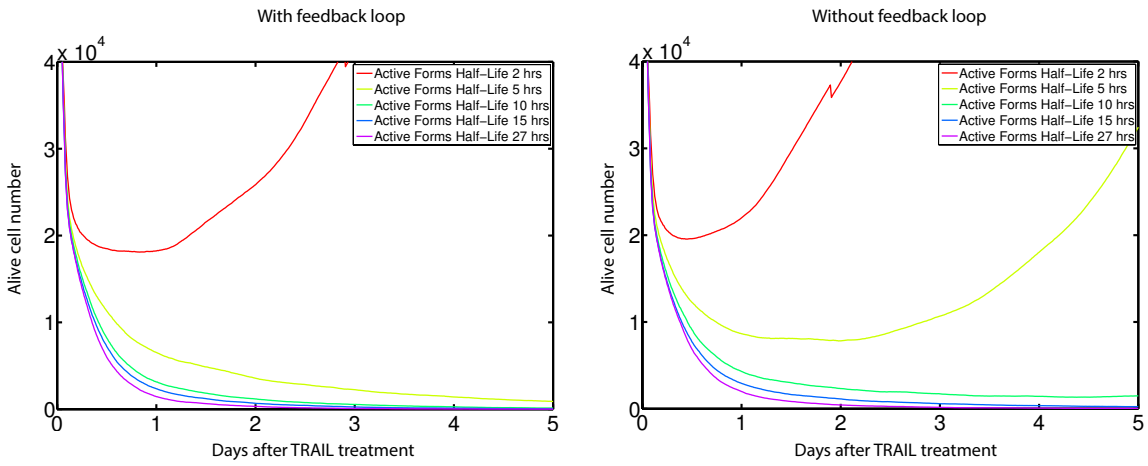

Figure S12: Long-term population survival is not possible with the feedback loop and stable active forms. Evolution of alive cell number in populations treated in-silico as in Fig. 6, for model several variants regarding presence/absence of the C3->C6->C8 feedback loop and the default active forms half-life.

Supplementary Methods

Simulating TRAIL-induced apoptosis with stochastic protein turnover

In general, the TRAIL signaling protein-protein reactions are taking place concurrently with stochastic protein turnover. When the noise in signaling reactions is neglected due to high protein copy number, those reactions can be simulated using ODEs. However, rates of protein synthesis are in our model stochastic, as they follow mRNA fluctuations.

Promoter activity and mRNA fluctuations were simulated using an implementation of the Gillespie algorithm in C++ (Numerical Recipes). Messenger RNA trajectories were computed and stored in advance because protein levels do not affect the rates of promoter state switches, mRNA production and degradation. The ODEs governing evolution of all protein levels were then simulated using the Semi-Implicit Extrapolation method implemented in C++ ([sup. ref. 15], Numerical Recipes). This method was significantly faster than a more standard Runge-Kutta method (Dormand-Prince, C++, Numerical Recipes) but gave identical results.

In-silico sister cells experiment

To sample the state (promoter activity, mRNA and protein levels) of the mother cells, all stochastic protein turnover models were simulated during 25 days (Monte-Carlo sampling) for each of the 10^4 (10^5 for results presented in main text) mother cells. This duration was verified by comparison with analytical results to be sufficient to reach the steady-state distribution. Sister cells were simply constructed by duplication of the mother cell state.

Because in experiments from [13], the distribution of durations between division and treatment was not uniform (see Figs. S5-b and 1-g in [13]), we applied a sampling algorithm to approximately reproduce those distributions. The overall impact on correlation curves was generally low compared to results obtained with assuming a fully uniform distribution of division time in the pre-stimulus recording interval. MOMP was considered to have occurred when half of mitochondrial Smac has been released.

In-silico repeated TRAIL experiment

A naïve population of 10^4 cells was obtained as in the sister cells experiment. Each cell was assigned a random time of next division. To account for the fact that the distribution of next division times is not uniform in growing cell populations, we used a distribution obtained by simulating simple growth. New cells were attributed a next division time according to a cell cycle duration normally distributed with 27 hours mean and 3 hours standard deviation. Cells in which cPARP levels exceeded 10^5 were considered dead as in [25]. To closely mimic the

experimental protocol used in [14], we accounted for the effect of passing cells by checking population size each day and if needed, removing randomly cells until 10^4 were left. Resistance gain is computed as $RG = \frac{Resistance^{survivors}}{Resistance^{naive\dagger cells}}$ where $Resistance = \frac{AliveCellNumber\left(treatment + 8hours\right)}{AliveCellNumber\left(treatment\right)}$, similarly to [14].

Quantification of model-data agreement

For the estimation Flip/Mcl1 model rates based cell fate variability experimental data, for the validation against transient cell fate inheritance data and for robustness analysis (Figs. 5A-C, 5E), it is needed to quantify the agreement/discrepancy between each model tested and the observed data. Such quantification was performed as follows:

- MOMP time distribution

Data was extracted from [13] (Fig. S4 b and c). It consists in MOMP time histograms (number of cells which did MOMP in a given 20 minutes time interval between 0 and 8 hours after treatment, 24 intervals in total). It was transformed in MOMP time frequencies by dividing by the total cell number. The same MOMP time frequencies were computed from simulated results. An agreement cost was then computed as the squared deviation between the two sets of frequencies, which respectively represent the empirical/model MOMP time distributions.

- Surviving fraction

An agreement cost for surviving fractions was simply computed as the squared difference between the surviving fractions observed experimentally and in simulations 8 hours after treatment.

- Sister cell MOMP time correlation curve

Spencer et al. [13] quantified the transient inheritance of MOMP times by computing a curve of sister cells MOMP time correlation as follows: pairs of sister cells for which both cells did MOMP before 8 hours were sorted as a function of the average time between division and MOMP, and linear regression correlation coefficients were computed for all groups obtained by sliding a window of constant size along the sorted pairs. For each group, mean time between division and MOMP was also computed, thus providing the abscissa of the corresponding point in the curve. From this data (Figs. S5-d in [13]), twenty representative points were extracted. To compute a comparable curve from simulations results, we applied the same quantification of sister cell MOMP time correlations. The group size was chosen

such that fraction of total pairs in each group is 10%, similarly to what has been done in [13]. One should not that the correlation values are available at different time points between the experimental and simulated curves. Thus, to permit a quantification of the agreement cost, each point in the experimental curve was mapped to the point in the simulated curve for which time points are the closest. The cost then penalizes, for each pair of points, a difference in the correlations but also in the time. In a formal manner, if for each point i in the data curve, the point $j = closestDivToMOMP_i$ in the simulated curve such that $DivToMOMP_j^{simulation}$ is the closest to $DivToMOMP_i^{data}$, the cost is then computed as:

$$cost = \sum \left(Corr_i^{data} - Corr_{closestDivToMOMP(i)}^{simulation} \right)^2 + \sum \left(DivToMOMP_i^{data} - DivToMOMP_{closestDivToMOMP(i)}^{simulation} \right)^2$$

- Comparison between the different types of data

To permit comparison between the different types of data, in each case a threshold for the cost defining agreement/disagreement was manually set by visual comparison of experimental and simulated data. For visualization purposes, Fig. 5-A,B,E represent a linearly normalized cost such that the threshold value correspond to 0.5 (represented in yellow). Normalized costs above 1 are capped to 1 and represented in red. The threshold costs used were 0.01/0.01, 0.01/0.01, and 2/2.5 for MOMP time distributions, surviving fractions and sister cell correlations respectively (TRAIL+CHX condition/TRAIL alone condition). To assign an agreement cost for MOMP time distribution AND surviving fractions (Fig. 5C), the maximum of the two normalized costs is taken.

Supplementary References

[1] F. C. Kischkel, S. Hellbardt, I. Behrmann, M. Germer, M. Pawlita, P. H. Krammer, and M. E. Peter, "Cytotoxicity-dependent APO-1 (Fas/CD95)-associated proteins form a death-inducing signaling complex (DISC) with the receptor.," *EMBO J.*, vol. 14, no. 22, pp. 5579–5588, Nov. 1995.

[2] Q. L. Deveraux, N. Roy, H. R. Stennicke, T. Van Arsdale, Q. Zhou, S. M. Srinivasula, E. S. Alnemri, G. S. Salvesen, and J. C. Reed, "IAPs block apoptotic events induced by caspase-8 and cytochrome c by direct inhibition of distinct caspases.," *EMBO J.*, vol. 17, no. 8, pp. 2215–2223, Apr. 1998.

[3] X. Luo, I. Budihardjo, H. Zou, C. Slaughter, and X. Wang, "Bid, a Bcl2 interacting protein, mediates cytochrome c release from mitochondria in response to activation of cell surface death receptors," *Cell*, vol. 94, no. 4, pp. 481–490, 1998.

[4] H. Kim, M. Rafiuddin-Shah, H.-C. Tu, J. R. Jeffers, G. P. Zambetti, J. J.-D. Hsieh, and E. H.-Y. Cheng, "Hierarchical regulation of mitochondrion-dependent apoptosis by BCL-2 subfamilies.," *Nat. Cell Biol.*, vol. 8, no. 12, pp. 1348–1358, Dec. 2006.

[5] C. Du, M. Fang, Y. Li, L. Li, and X. Wang, "Smac, a mitochondrial protein that promotes cytochrome c-dependent caspase activation by eliminating IAP inhibition.," *Cell*, vol. 102, no. 1, pp. 33–42, Jul. 2000.

[6] B. Schwanhäusser, D. Busse, N. Li, G. Dittmar, J. Schuchhardt, J. Wolf, W. Chen, and M. Selbach, "Global quantification of mammalian gene expression control," *Nature*, vol. 473, no. 7347, pp. 337–342, May 2011.

[7] L. V. Sharova, A. A. Sharov, T. Nedorezov, Y. Piao, N. Shaik, and M. S. H. Ko, "Database for mRNA Half-Life of 19 977 Genes Obtained by DNA Microarray Analysis of Pluripotent and Differentiating Mouse Embryonic Stem Cells," *DNA Research*, vol. 16, no. 1, pp. 45–58, Jan. 2009.

[8] Y. S. Youn, M. J. Shin, S. Y. Chae, C.-H. Jin, T. H. Kim, and K. C. Lee, "Biological and physicochemical evaluation of the conformational stability of tumor necrosis factor-related apoptosis-inducing ligand (TRAIL)," *Biotechnol Lett*, vol. 29, no. 5, pp. 713–721, Feb. 2007.

[9] K. Breitschopf, "Ubiquitin-mediated Degradation of the Proapoptotic Active Form of Bid. A Functional Consequence on Apoptosis Induction," *Journal of Biological Chemistry*, vol. 275, no. 28, pp. 21648–21652, May 2000.

[10] E. Ferraro, A. Pulicati, M. T. Cencioni, M. Cozzolino, F. Navoni, S. di Martino, R. Nardacci, M. T. Carrì, and F. Cecconi, "Apoptosome-deficient cells lose cytochrome c through proteasomal degradation but survive by autophagy-dependent glycolysis.," *Mol. Biol. Cell*, vol. 19, no. 8, pp. 3576–3588, Aug. 2008.

[11] B. Li and Q. P. Dou, "Bax degradation by the ubiquitin/proteasome-dependent pathway: involvement in tumor survival and progression.," *Proc. Natl. Acad. Sci. U.S.A.*, vol. 97, no. 8, pp. 3850–3855, Apr. 2000.

[12] P. Tawa, K. Hell, A. Giroux, E. Grimm, Y. Han, D. W. Nicholson, and S. Xanthoudakis, "Catalytic activity of caspase-3 is required for its degradation: stabilization of the active complex by synthetic inhibitors.," *Cell Death Differ.*, vol. 11, no. 4, pp. 439–447, Apr. 2004.

[13] J. A. Thorpe, P. A. Christian, and S. R. Schwarze, "Proteasome inhibition blocks caspase-8 degradation and sensitizes prostate cancer cells to death receptor-mediated apoptosis," *Prostate*, vol. 68, no. 2, pp. 200–209, 2007.

[14] M. Bushell, M. Stoneley, Y. W. Kong, T. L. Hamilton, K. A. Spriggs, H. C. Dobbyn, X. Qin, P. Sarnow, and A. E. Willis, "Polypyrimidine tract binding protein regulates IRES-mediated gene expression during apoptosis.," *Molecular Cell*, vol. 23, no. 3, pp. 401–412, Aug. 2006.

[15] P. Deuflhard, "Recent Progress in Extrapolation Methods for Ordinary Differential Equations," *SIAM Rev.*, vol. 27, no. 4, pp. 505–535, Dec. 1985.